Vitamin D-conjugated gold nanoparticles as functional carriers to enhancing osteogenic differentiation

Haram Nah, Donghyun Lee, Min Heo, Jae Seo Lee, Sang Jin Lee, Dong Nyoung Heo, Jeongmin Seong, Ho-Nam Lim, Yeon-Hee Lee, Ho-Jin Moon, Yu-Shik Hwang & Il Keun Kwon

Taylor & Francis
Taylor & Francis Group

Vitamin D-conjugated gold nanoparticles as functional carriers to enhancing osteogenic differentiation

Haram Nah [ID] [a*], Donghyun Lee [ID] [b,c*], Min Heo [b], Jae Seo Lee [ID] [a], Sang Jin Lee [ID] [b], Dong Nyoung Heo [ID] [b], Jeongmin Seong [d], Ho-Nam Lim [b], Yeon-Hee Lee [e], Ho-Jin Moon [ID] [b], Yu-Shik Hwang [f] and Il Keun Kwon [ID] [b]

[a]Department of Dentistry, Graduate School, Kyung Hee University, Seoul, Republic of Korea;
[b]Department of Dental Materials, School of Dentistry, Kyung Hee University, Seoul, Republic of Korea;
[c]Laboratory Animal Center, Daegu-Gyeongbuk Medical Innovation Foundation, Daegu, Republic of Korea;
[d]Department of Dental Hygiene, College of Health Science, Kangwon National University, Samcheok-si, Republic of Korea;
[e]Department of Orofacial Pain and Oral Medicine, School of Dentistry, Kyung Hee University, Seoul, Republic of Korea;
[f]Department of Maxillofacial Biomedical Engineering, School of Dentistry, Kyung Hee University, Seoul, Republic of Korea

ABSTRACT

In an aging society, bone disorders such as osteopenia, osteoporosis, and degenerative arthritis cause serious public health problems. In order to solve these problems, researchers continue to develop therapeutic agents, increase the efficacy of developed therapeutic agents, and reduce side effects. Gold nanoparticles (GNPs) are widely used in tissue engineering applications as biosensors, drug delivery carriers, and bioactive materials. Their special surface property enables easy conjugation with ligands including functional groups such as thiols, phosphines, and amines. This creates an attractive advantage to GNPs for use in the bone tissue engineering field. However, GNPs alone are limited in their biological effects. In this study, we used thiol-PEG-vitamin D (SPVD) to conjugate vitamin D, an essential nutrient critical for maintaining normal skeletal homeostasis, to GNPs. To characterize vitamin D-conjugated GNPs (VGNPs), field emission transmission electron microscopy, energy dispersive X-ray spectroscopy, dynamic light scattering, and ultraviolet/visible absorption analysis were carried out. The developed VGNPs were well bound through the thiol groups between GNPs and vitamin D, and were fabricated in size of 60 nm. Moreover, to demonstrate VGNPs osteogenic differentiation effect, various assays were carried out through cell viability test, alkaline phosphatase assay, calcium deposition assay, real-time polymerase chain reaction, and immunofluorescence staining. As a result, the fabricated VGNPs were found to effectively enhance osteogenic differentiation of human adipose-derived stem cells (hADSCs) *in vitro*. Based on these results, VGNPs can be utilized as functional nanomaterials for bone regeneration in the tissue engineering field.
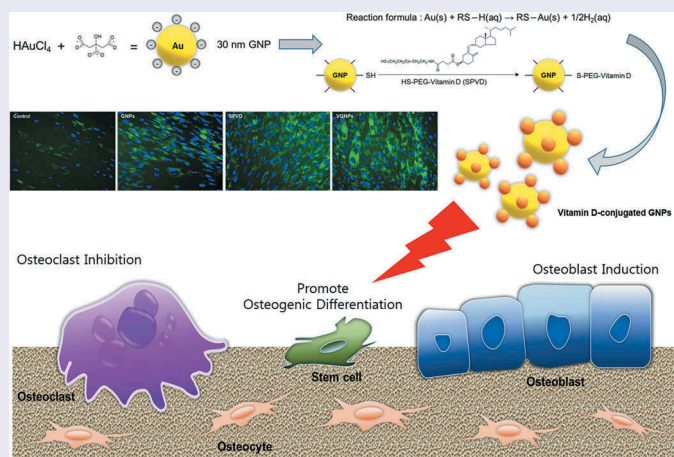
1. Introduction

Bone is an important organ that plays several key roles in human including protection, movement, support of other organs, and blood production as well as other roles [1]. The importance of maintaining healthy bone status is clear for both clinical and economic reasons.

For instance, more than 1 million bone related surgical procedures, such as bone grafting and fracture repair, are performed in the United States at an estimated cost of more than $5 billion every year [2]. Especially, osteoporosis, which is one of the major causes of bone disorders affecting one-eighth of men and one-third of women over the age of 50 worldwide [3]. According to the International Osteoporosis Foundation, 2 million osteoporotic fractures occurred annually in the United States and 3.5 million in the European Union [4]. Due to longer life expectancies, bone health is increasing in importance for society. This concern will continually grow in the future. Consequentially, the necessity of a new osteogenic agent that more effectively enhances bone formation with no side effects is critical.

Besides traumas, the most common contributing factors to bone fractures originate from structural exacerbation of bones and their low bone mineral density. Vitamin D is a well-known essential nutrient to the human body that is obtainable from supplements, diet, and sun exposure [5]. Synthesis of vitamin D occurs after exposure to sunlight through the liver or the kidney or it is obtained from the diet. The active vitamin D metabolite, 1α, 25-dihydroxyvitamin D_3 (1,25$(OH)_2D_3$), assumes a vital function in skeletal homeostasis by regulating intestinal absorption of calcium and phosphate [6,7]. In addition, the active form of vitamin D plays a role in inhibition of osteoclastogenesis [8]. On the other hand, deficiency of vitamin D contributes to rickets in children and osteomalacia in adults [9]. Song et al. [10] investigated the osteogenic differentiation of human recombinant bone morphogenetic protein-2 (BMP-2) and vitamin D on adipose stem cells. Piek et al. [11] reported that vitamin D strongly improves the expression of genes on human mesenchymal stem cells as an enhancer of BMP-2-induced osteogenesis. However, adequate intake of vitamin D is not easy for modern people who are customarily indoors. Therefore, many researchers have attempted delivery of vitamin D through nanoparticles [12].

Over the past decade, 'nano' sized vehicles are generally being utilized as drug carriers in biomedical applications. These come in various forms comprising of polymers, dendrimers, liposomes, nanotubes, and nanorods [13–15]. Amongst these various platforms, Gold nanoparticles (GNPs), one of the most promising nanoparticle-based colloidal carriers, have been widely investigated in numerous fields such as tissue engineering, biochemistry, biotechnology, and nanomedicine [14,16]. GNPs have many benefits, due to their unique physicochemical properties, such as high surface area to volume ratio, small size, and solubility [17–19]. The most attractive advantage of GNPs is tunable surface modifications. Ligands, including functional groups such as thiols, phosphines, and amines, exhibit an affinity for gold

surfaces and can be readily used to modify GNPs surfaces [14,20]. Recently, researchers focused on how various applications of GNPs could be used to enhance osteogenic effects. Lee et al. [21] reported that GNPs-combined with poly(lactide-co-glycolide) (PLGA) nanofibrous scaffolds demonstrated an osteogenic effect. GNPs could be bound to thiolated PLGA through their surface interaction with thiol groups. Heo et al. [22] reported that GNPs enhance osteogenic differentiation in a manner similar to BMP-2 when applied to methacrylated gelatine hydrogel. In this regard, it has been found that GNPs-based systems can affect osteogenic differentiation and are suitable materials for use in bone tissue engineering applications.

To synthesize vitamin D-conjugated GNPs, which are expected to have a synergistic effect for bone regeneration as functionalized carriers, we used strong chemical bonding between gold and thiol moieties [20]. Thiol-functionalized polyethylene glycol conjugated-vitamin D (SPVD) was used to combine with GNPs. The PEG linkage was used as this provides for more steric stability with reduced nanoparticle aggregation and breakdown during blood circulation in the human body [23].

In this work, we synthesized SPVD-conjugated GNPs (VGNPs) to enable enhanced osteogenesis. Field emission transmission electron microscopy (FE-TEM), energy dispersive X-ray spectroscopy (EDS), dynamic light scattering (DLS), and UV-Visible spectroscopy (UV-vis) were used to comprehensively characterize the VGNPs. A cell viability test was performed against human adipose-derived stem cells (hADSCs) to ensure that the concentrations applied were not cytotoxic. To confirm the intracellular uptake properties, dark field assays were also performed. Osteogenic differentiation of hADSCs was evaluated by alkaline phosphatase (ALP) activity, calcium deposition assay, real-time polymerase chain reaction (real-time PCR), and immunofluorescence staining (IF).

2. Materials and methods

2.1. Materials

Gold(III) chloride hydrate (99.999% trace metals basis), sodium citrate, β-glycerol phosphate disodium salt hydrate, ascorbic acid, and dexamethasone were purchased from Sigma-Aldrich (St. Louis, MO, USA). Human adipose tissue-derived MSC, CEFOgro™ ADMSC Human Adipose tissue-derived MSC Growth Medium, and CEFOgro™ ADMSC Supplement (10% FBS, 0.02% Penicillin & Streptomycin) were purchased from CEFO Co. Ltd. (Seoul, Korea). EZ-Cytox (enhanced cell viability assay kit) was purchased from Dogen (Seoul, Korea). Dulbecco's modified eagle

medium (DMEM), fetal bovine serum (FBS), penicillin and streptomycin (PS), TrypLE^TM Express, and Dulbecco's phosphate buffered saline (DPBS) were purchased from GIBCO (Grand Island, NY, USA). PG2-THVD-3k was purchased from NANOCS (New York, NY, USA).

2.2. Synthesis of GNPs and VGNPs

Aqueous dispersions of GNPs were synthesized by citrate reduction of $HAuCl_4$ [24,25]. To synthesize 30 nm GNPs, 0.02% $HAuCl_4$ solution (800 mL) was refluxed, and then 2% sodium citrate solution (15 mL) was quickly added into the flask. Each solution was dissolved in distilled water. The color of the solution changed from yellow to deep purple. Afterwards, the solution was stirred until it reached room temperature overnight, and then was filtered using a 0.22 μm filter (Millipore, Carrigtwohill, Ireland). After synthesis, the GNPs were stored in distilled water suspension at 4°C. The fabricated GNPs generated by citrate reduction method had an average size of 30 nm (Figure 1(a)) [25]. To conjugated vitamin D with GNPs, SPVD was dissolved at 5 mg/mL in distilled water and stored at −20°C. VGNPs were fabricated such that a 1:1 volume ratio of each GNPs and SPVD solution were vigorously stirred in room temperature during 24 h.

2.3. Synthesized VGNPs characterization

The synthesized GNPs and VGNPs were observed by FE-TEM (JEM-2100F, JEOL, Japan) to identify the morphology of VGNPs. The GNPs and VGNPs solutions were dropped onto a 200-mesh copper grid coated with Formvar/carbone (Ted Pella Inc., Redding, USA) and dried under vacuum at room temperature. After complete drying, the GNPs and VGNPs were imaged at 100 kV. EDS (51-XMX1034, Oxford, UK) peaks were analyzed based on a region of the surface of GNPs and VGNPs, with the same observation conditions of FE-TEM. The particles diameters and degree of dispersions of the GNPs and VGNPs were measured by DLS (ELSZ-1000, Photal Otsuka Electronics, Japan). The GNPs and VGNPs solutions were diluted to a concentration of 100 μM

for analysis. The stability of synthesized SPVD on the GNPs was confirmed by UV-vis (UV-1650PC, Shimadzu Europe, Germany). The prepared GNPs and VGNPs solutions were measured at a concentration of 20 μM in colloidal solution states.

2.4. hADSCs culture and viability test

The hADSCs were cultured in CEFOgro^TM ADMSC Human Adipose tissue-derived MSC Growth Medium containing CEFOgro^TM ADMSC Supplement (10% FBS, 0.02% Penicillin & Streptomycin) (growth medium (GM)) or DMEM containing 10% FBS, 1% PS, 10 mM β-glycerol phosphate disodium salt hydrate, 300 μM ascorbic acid, and 0.1 μM dexamethasone (osteogenic medium (OM)) in a 5% CO_2/37°C incubator (Isotemp, Thermo Fisher Scientific). The GM and OM were replaced every 3 days in all cell experiments using hADSCs. The hADSCs were dived into groups including non-treated (control), 20 μM GNPs treated, 20 μM SPVD treated, and 20 μM VGNPs treated groups. Each group was seeded onto a 24-well culture plate at a seeding density of 5×10^4 cells/well (n = 4) including GM. EZ-Cytox was used to evaluate optical densities of hADSCs. At 1, 3, and 7 days of evaluations, hADSCs seeded in 24-well culture plates were washed by DPBS and were treated EZ-Cytox solution. This was diluted using free GM including no supplements at a ratio of 1:10. After 2 h of incubation, the intensity was measured by a microplate reader (BioRad, Hercules, USA) at a wavelength of 450 nm.

2.5. Dark-field assay

hADSCs (a density of 2×10^4 cells/well) were seeded on a 10 mm confocal dish (SPL, Seoul, Korea) with GM and incubated 2 h to allow for cell attachment. After 2 h, the medium was changed to a new medium containing 20 μM GNPs or 20 μM VGNPs and then incubated for 24 h. After removing the medium, the cells were washed with DPBS twice, fixed in 3.7% formaldehyde at room temperature for 30 min, and were then washed with DPBS twice again. The cells were examined by optical microscope (DM2500,
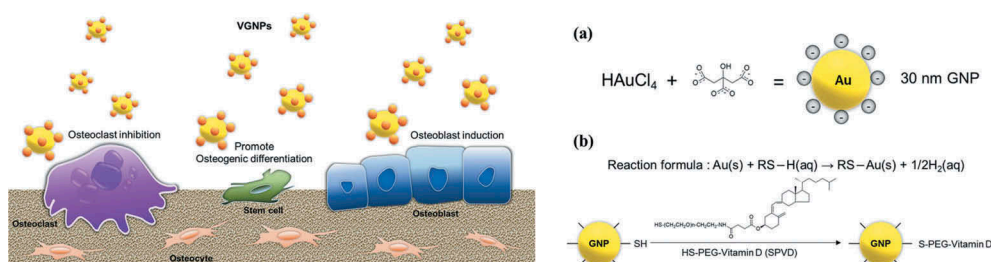

Figure 1. Schematic illustration of the vitamin D-conjugated gold nanoparticles (VGNPs). Reaction scheme showing the synthesis of GNPs (a), and VGNPs (b).

Leica, Germany). Image J program was used for analyzing the images of GNPs and VGNPs for intracellular uptake. The total bright spots in the whole area were analyzed to calculate the amount of intracellular uptake. The uptake ratio was calculated by using Image-J program.

2.6. Alkaline phosphatase (ALP) activity

hADSCs (a density of 5×10^4 cells/well) were seeded on 24-well culture plates (n = 4), and incubated in OM containing each 20 μM GNPs, SPVD, and VGNPs for 5, 10, and 15 days, respectively. The cells seeded in the wells were washed with DPBS twice and lysed by 1x RIPA buffer (50 mM Tri-HCL (pH 7.4.)), 150 mM NaCl (0.25% deoxycholic acid, 1% NP-40 and 1 mM EDTA) with a protease inhibitor cocktail (Boehringer Mannheim GmbH, Germany) for 1 h on ice. After 1 h, each group of lysates was collected into the 1.5 mL tubes. The supernatant was collected and then reacted with p-nitrophenyl phosphate solution (pNPP, sigma) at room temperature for 30 min. The reaction with pNPP was then terminated by adding 50 μL of 1 M NaOH. The production of p-nitrophenol was measured by absorption at 450 nm using a microplate reader. A calibration curve was generated using standard p-nitrophenol solutions. The quantity of produced total p-nitrophenol from cultured cells was obtained by comparing their results against a calibration curve. Finally, the enzyme activity was expressed as μM of reaction product (p-nitrophenol) per minute per μg of total cellular protein.

2.7. Calcium deposition assay

hADSCs (a density of 5×10^4 cells/well) were seeded on 24-well culture plates (n = 4), and incubated in OM containing each 20 μM GNPs, SPVD, or VGNPs for 1, 2, and 3 weeks, respectively. The cells seeded in the wells were washed with DPBS twice and fixed in 3.7% formaldehyde at room temperature for 30 min. After fixation, the cells were washed with DPBS twice again and treated with 40 mM alizarin red staining solution (pH 4.2) for 30 min. The solution was removed after 30 min, washed with distilled water, and then examined using a microscope digital camera (IX71, OLYMPUS, Japan). For a quantitative analysis of calcium deposition, the stained cells were desorbed with 10% cetylpyridinium chloride. The absorbance was measured by using a microplate reader at 540 nm.

2.8. Real-time polymerase chain reaction (real-time PCR)

hADSCs were seeded on 24-well culture plates at a density of 5×10^4 cells/well density. These were incubated in each of non-treated OM (control), 20 μM GNPs treated OM, 20 μM SPVD treated OM, and 20 μM VGNPs treated OM for 1, 2, and 3 weeks, respectively. Each non-treated or treated medium was changed every 3 days during the culture periods. At each predetermined time period, the seeded hADSCs were washed with DPBS one time and the entire RNA from all samples was isolated using TRIzol™ Reagent (Invitrogen, Waltham, USA) according to manufacturer's instructions. 1 μg of total RNA was extracted from whole samples and transcribed into cDNA using an AccuPower Cycle Script RT Premix (Bioneer, Daejeon, Republic of Korea). IQ SYBR Green supermix (Bio-Rad, Hercules, USA) was used to analyse real-time PCR. The primers of the analysed mRNA genes are as shown in Table 1. Threshold cycle values were calculated by using a comparative cycle threshold method. The fold change of the control group (osteogenic differentiation medium only) at 7 days of culture was set as 1-fold and the ratio of the normalized fold change was calculated. The amplifications of real-time PCR were carried out for 10 seconds at 95°C, 30 seconds at 53–57°C (Collagen type 1 (COL1): 53°C, osteopontin (OPN): 56°C, bone morphogenetic protein-2 (BMP-2): 57°C, bone sialoprotein (BSP): 54°C and 30 seconds at 72°C for 45 cycles after the initial denaturation step for 10 minutes at 95°C. The primers used in analysis were purchased from Bioneer (Daejeon, Republic of Korea). All results from real-time PCR were normalized by GAPDH.

2.9. Immunofluorescence staining (IF) analysis

hADSCs (at a density of 5×10^4 cells/well) were seeded on 24-well culture plates (n = 4) and incubated in OM containing 20 μM GNPs, SPVD, or VGNPs for 10 days. The cells were washed with DPBS and fixed in 3.7% formaldehyde at room temperature for 30 min. They were then washed with DPBS twice again. After washing, the cells were permeabilized with 0.1% Tween #20 (Yakuri Pure Chemicals Co. Ltd., Kyoto, Japan) for 10 min and blocked with 1% bovine serum albumin (Sigma-Aldrich, St. Louis, USA) in PBS (GIBCO, Grand Island, USA) for 1 h at 4°C. A monoclonal anti-osteocalcin antibody (sc-74495, Santa Cruz, USA)

Table 1. The sequences of human osteogenic primer used for real-time PCR.

Primers		Sequence (5'-3')
COL1	Forward	ATGACTATGAGTATGGGGAAGCA
	Reverse	TGGGTCCCTCTGTTACACTTT
OPN	Forward	CCCTTCCAAGTAAGTCCAACGAAAGC
	Reverse	CTGGATGTCAGGTCTGCGAAACTTC
BMP-2	Forward	TGGCCCACTTGGAGGAGAAACA
	Reverse	CGCTGTTTGTGTTTGGCTTGACG
BSP	Forward	AACGAAGAAAGCGAAGCAGAA
	Reverse	TCTGCCTCTGTGCTGTTGGT
GAPDH	Forward	AGCCACATCGCTCAGACAC
	Reverse	GCCCAATACGACCAAATGG

was used at a dilution of 1:100. Goat anti-mouse IgG-PE (sc-3738, Santa Cruz, USA) secondary antibody was used at a dilution of 1:500. Nuclei were stained with 2-(4-Amidinophenyl)-6-indolecarbamidine dihydrochloride (Sigma-Aldrich, St. Louis, USA). The cells were examined by microscope digital camera.

2.10. Statistical analysis

All experiments with hADSCs were seeded in four-wells per group in order to perform quantifiable analysis. Two-way ANOVA with Tukey's multiple comparison post-hoc test was used to perform statistical analysis. All values are expressed as mean ± standard deviation, and all the experimental groups are compared with each other. Significance was defined as *$p < 0.05$, **$p < 0.01$, and ***$p < 0.001$.

3. Results

3.1. Synthesis and characterization of VGNPs

In the FE-TEM images (Figure 2(a)), both GNPs and VGNPs groups showed a similar spherical morphology with no significant differences. The fabricated GNPs and VGNPs were of uniform dose distribution, however, GNPs showed a narrower interparticle distance than VGNPs. In the magnification of × 300,000 images, both of GNPs and VGNPs had 30–40 nm diameters in dry state.

The diameter and uniformity of the GNPs and VGNPs were precisely measured by DLS. The results of DLS analysis confirmed that the diameters of VGNPs were 1.6 times longer than GNPs, unlike the results of the TEM images. In addition, the polydispersity index (PDI) values of each of GNPs and VGNPs were 0.29 ± 0.03 and 0.29 ± 0.02 (Table 2), respectively. Consequently, the synthesized VGNPs' degree of dispersity was shown to be highly uniform in a colloidal solution state.

Table 2. Mean diameter and polydispersity measured by DLS for GNPs and VGNPs. Data are provided as mean ± standard deviation (n = 4).

	Mean Diameter (nm)	Polydispersity (PDI)
GNPs	36.5 ± 1.1	0.29 ± 0.03
VGNPs	60.8 ± 0.3	0.29 ± 0.02

Table 3. EDS results of the GNPs and VGNPs.

	Weight%		Atomic%	
Element	GNPs	VGNPs	GNPs	VGNPs
Au	100	99.7	100	98.1
S	0	0.3	0	1.9

The EDS results indicated that synthesized VGNPs had elemental S components originating from bonding between the GNPs surface and the – SH groups of SPVD. The quantified EDS results indicated that VGNPs had 0.32 weight percentages and 1.93 atomic percentages of sulfur (Table 3). UV-vis spectra of the particles are shown in Figure 2(d). Maximum absorbance in GNPs and SPVD was observed at 526 and 530 nm, respectively. The spectral shape was similar but shifted to a longer wavelength for SPVD.

3.2. Biocompatibility of VGNPs on hADSCs

The cell viability test on hADSCs, which had been cultured for 1, 3, and 7 days with 20 μM GNPs treated GM, 20 μM SPVD treated GM, and 20 μM VGNPs treated GM. These results were compared with non-treated GM (control). In order to quantify, we measured the cell viability percentage among groups using the EZ-Cytox (Figure 3(a)). All treated GM groups showed higher cell viability than control group after 3 days of culture. All the VGNPs treated GM groups indicated higher cell viability than control group during 7 days of culture. In addition, VGNPs treated GM group's cell viability level was superior as compared to both GNPs treated group
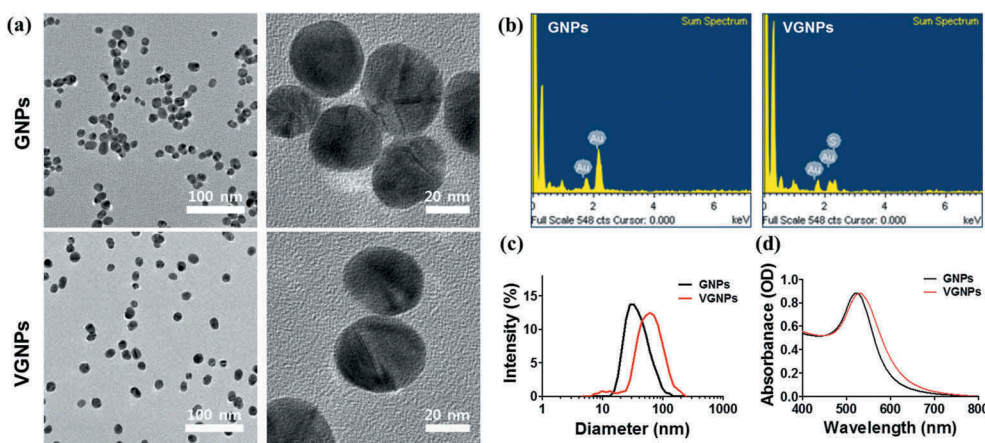

Figure 2. Structure and characterization of GNPs and VGNPs: FE-TEM images of the GNPs and VGNPs (a). EDS analysis results of GNPs and VGNPs (b). Size distribution of GNPs and VGNPs, as measured by DLS (c). Surface plasmon absorption spectra of GNPs and VGNPs (d). Scale bars are 100 nm and 20 nm.

and SPVD treated group. These results indicate that 20 μM of VGNPs has no significant cytotoxicity toward hADSCs.

3.3. Intracellular uptake of VGNPs on hADSCs

To identify the intracellular uptake properties of synthesized GNPs and VGNPs, dark field microscopy observations were performed (Figure 4). The hADSCs that were seeded onto a confocal dish were incubated for 2 h in order to stably attach to the culture plate. After that, these were treated with 20 μM GNPs or VGNPs in GM for 24 h. All samples were observed under bright or dark field imaging conditions. In the dark field images, the intracellular uptake GNPs or VGNPs were displayed as bright spots. The hADSCs and particles were well dispersed throughout. The results showed that more white spots were observed in GNPs treated hADSCs (Figure 4(a)). As shown in Figure 4(b), the VGNPs treated samples showed lower uptake ratio than GNPs treated samples.

3.4. Osteogenic differentiation effects of VGNPs on hADSCs

The ALP activity levels showing differentiation of hADSCs toward osteoblasts were examined. This was performed with hADSCs cultured on 24-well culture plates for 5, 10 and 15 days with osteogenic medium containing no treatment (control) as well as GNPs, SPVD, or VGNPs at 20 μM concentrations, each respectively. The SPVD and VGNPs groups were observed to have higher ALP levels than others (Figure 3(b)). SPVD treated groups showed slightly higher ALP level than VGNPs, however, there was no statistically significant difference. Both SPVD and VGNPs treated groups were found to have significantly higher ALP activity levels than control and GNPs treated groups. These results indicate that

VGNPs can positively affect the osteogenic differentiation of hADSCs.

3.5. Osteogenic differentiation effects of VGNPs on hADSCs

The calcium deposition was measured for hADSCs cultured on 24-well culture plates and incubated for 1, 2, and 3 weeks with osteogenic medium containing no treatment (control) as well as GNPs, SPVD, or VGNPs at 20 μM concentrations, respectively. The quantity of deposited calcium was compared to each group after alizarin red staining solution (Figure 5(a)). The calcium deposition increased during the 3 weeks of testing. In order to quantify the deposited calcium from each group, all groups were dissolved using 10% cetylpyridinium chloride. After dissolving, the optical density (O.D.) was measured by a microplate reader (Figure 5(b)). There was no significant difference over the first two weeks, but GNPs, SPVD, and VGNPs treated groups showed significant differences at week 3. The VGNPs treated groups showed the highest levels of calcium deposition and there was a statistically significant difference as compared to GNPs and SPVD treated groups. These results indicate that VGNPs strongly affect the osteogenic differentiation of hADSCs.

3.6. Osteogenic differentiation effects of VGNPs on hADSCs

The mRNA expressions of osteoblast gene markers such as COL1, OPN, BMP-2, and BSP were examined by real-time PCR (Figure 6). All results from gene markers were normalized to GAPDH expression. As shown in Figure 6(d), BSP, which is late osteoblastogenic marker, was observed at the highest levels of expressions at 3 weeks. All groups were observed to demonstrate higher expression levels as compared to control at 2 weeks and showed increasing activity
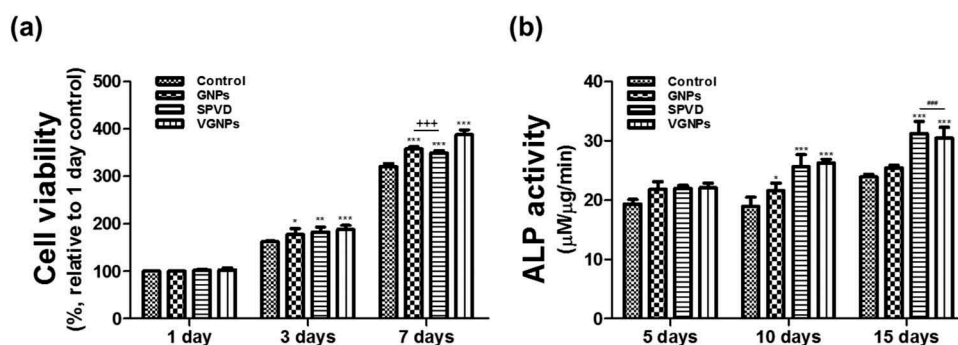

Figure 3. Evaluation of cell viability (a) and ALP activity (b) of hADSCs: cell viability performed after 1, 3, and 7 days of culture at non-treated GM (control), GNPs treated GM, SPVD treated GM, and VGNPs treated GM. ALP activity performed after 5, 10, and 15 days of culture at non-treated OM (control), GNPs treated OM, SPVD treated OM, and VGNPs treated OM. n = 4, *p < 0.05, **p < 0.01, and ***p < 0.001 compared with the control group, +++p < 0.001 compared with the VGNPs treated GM group, and ###p < 0.001 compared with the GNPs treated OM group.
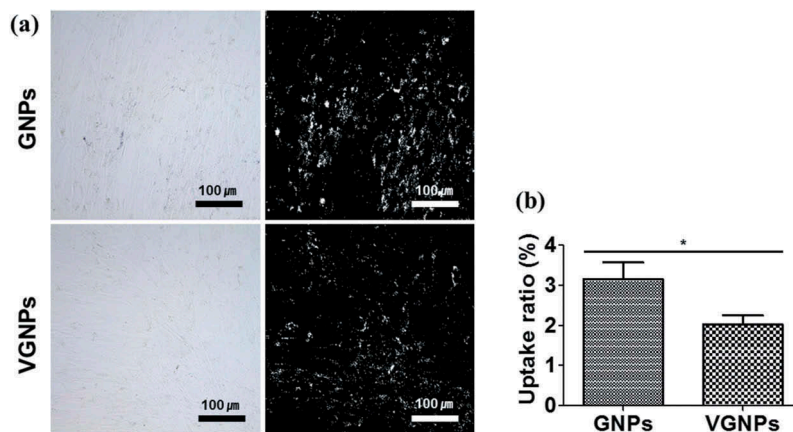
Figure 4. Optical images and dark field images of GNPs and VGNPs treated on hADSCs (a). The cellular uptake ration of GNPs and VGNPs treated hADSCs (b). For the quantitative analysis, the scattering images calculated by Image J program (bright area per total area), and the results are shown as mean ± standard deviation of triplicate experiments (n = 4). Scale bars are 100 μm.
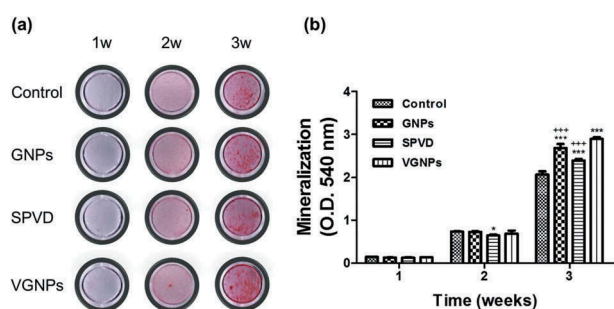

Figure 5. Alizarin red staining (a) and calcium deposition (b) of hADSCs. Calcium deposition tested after 1, 2, and 3 weeks of culture at non-treated OM (control), GNPs treated OM, SPVD treated OM, and VGNPs treated OM. n = 4, *p < 0.05, and ***p < 0.001 compared with the control group, +++p < 0.001 compared with the VGNPs treated OM group.

over the course of time. At 3 weeks, VGNPs displayed the highest expression levels of BSP mRNA expression as compared to the control group. Moreover, the VGNPs had higher expression not only compared to the control but also as compared to GNPs and SPVD groups. On the other hand, VGNPs displayed the highest expression of COL1, which is an early marker of osteogenic differentiation, at 2 weeks of culture (Figure 6(a)). In Figure 6(b), VGNPs displayed significantly higher OPN, which is the other early marker of osteoblastogenesis, as compared to both control and GNPs at 2 weeks. In particular, VGNPs showed significantly higher expression levels of OPN mRNA as compared to others at 1 week. All groups indicated BMP-2, which is an osteogenic transcription factor, expression levels with the highest expressions at 2 weeks among the whole time period of measurement (Figure 6(c)). The highest level of BMP-2 was found with VGNPs at 3 weeks. At 1 week, VGNPs displayed a significantly higher expression level of BMP-2 as compared to both control and GNPs. It was generally found that the

VGNPs showed the highest expression levels for all markers at all time periods.

3.7. Osteogenic differentiation effects of VGNPs on hADSCs

The cells were cultured for 10 days with osteogenic medium only, osteogenic medium containing each of GNPs, SPVD, or VGNPs (20 μM). Immunofluorescence staining was used to confirm the effect of GNPs, SPVD, and VGNPs on osteocalcin (OCN) expression of hADSCs. As demonstrated in Figure 7(d), GNPs, SPVD, and VGNPs groups showed significant increase in immunofluorescence staining of OCN when compared to the control group. While VGNPs group showed a slightly higher staining intensity when compared to SPVD group. The results indicated that GNPs, SPVD, and VGNPs promoted osteogenic differentiation whereby VGNPs had a more pronounced effect.

4. Discussion

GNPs are quite attractive on their own, and at the same time, serve as a material that finds extensive use in many biomedical applications such as clinical diagnostics, therapeutics, and theranostics [13,26]. In the process of bone regeneration, GNPs affect the activation of the p38 mitogen-activated protein kinase (MAPK) signaling pathway, promoting the osteogenic differentiation of mesenchymal stem cells (MSCs) [27]. Accordingly, we investigated the effect on bone regeneration of GNPs [21,22,28,29]. Our previous study determined GNPs with diameters of 30 and 50 nm to be effective for increasing osteogenic differentiations [28]. Based on this study, we designed a 30 nm diameter GNPs. We used the smaller size due to considerations regarding the diameter increase after conjugation with SPVD. Through the DLS
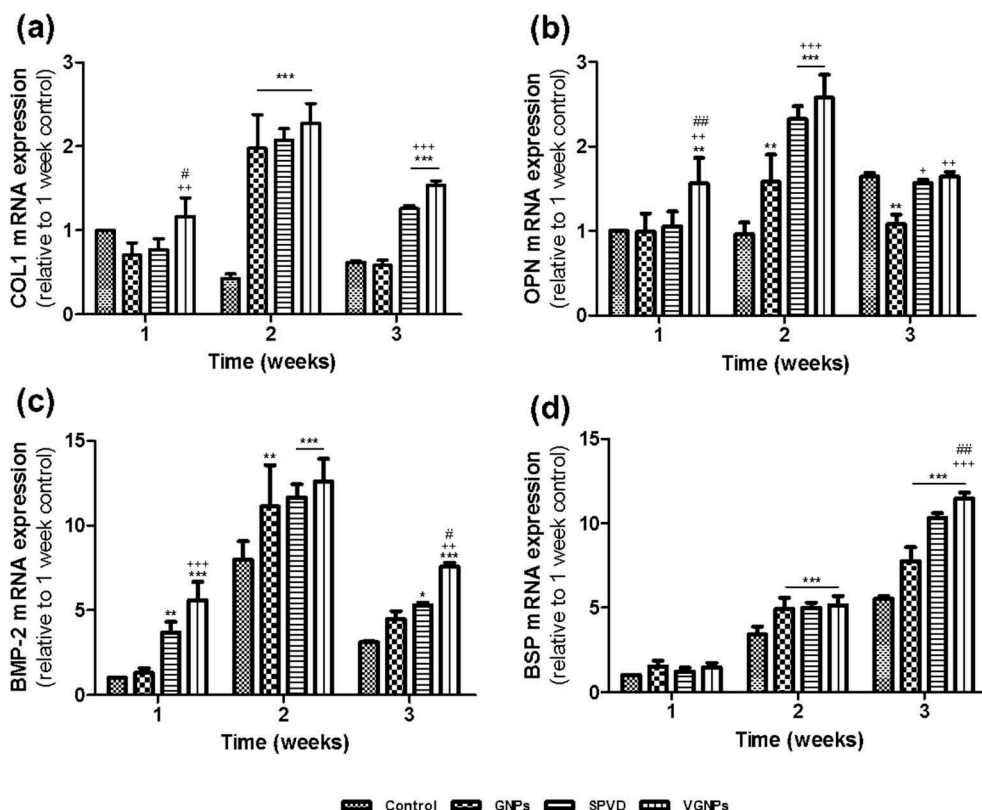
Figure 6. The mRNA expression of osteogenic markers during the process of differentiation for 1, 2, and 3 weeks: COL1 (a), OPN (b), BMP2 (c), and BSP (d). n = 4, *P < 0.05, **P < 0.01, and ***P < 0.001 compared to control group, +P < 0.05, ++P < 0.01, and +++P < 0.001 compared to GNPs group, and # P < 0.05, ## P < 0.01 compared to SPVD.
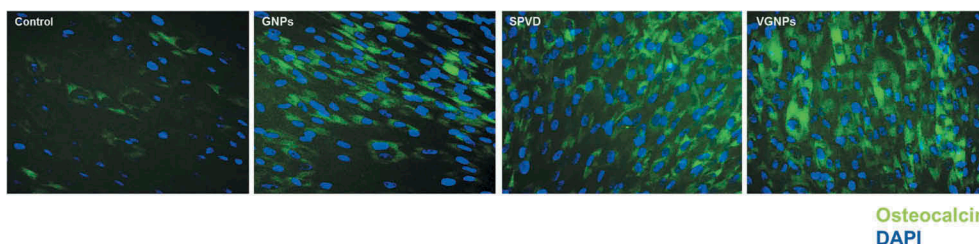

Figure 7. Detection of osteocalcin (OCN) immunofluorescence. After 10 days incubation of non-treated OM (control), GNPs treated OM, SPVD treated OM, and VGNPs treated OM, OCN immunofluorescence results were observed by optical microscopy. Green, OCN positive area; and blue, nuclei merged color of green and blue.

analysis, the diameter change after conjugation with SPVD was confirmed (Figure 2(c)). In the DLS results, the VGNPs diameter increased the GNPs size to 60.8 ± 0.3 nm. The PDI values of both GNPs and VGNPs were measured to be under 0.3. There is no specific 'good' value for PDI, however, a PDI below 1.0 is generally associated with a high homogeneity in the particle population [30]. Therefore, the fabricated VGNPs were well dispersed in the colloidal solution state (Table 2). A strong absorption peak due to VGNPs was found by UV/Vis analysis (Figure 2(d)). The addition of vitamin D shifted the absorption peak of GNPs from 526 nm to 530 nm. This peak shift appears to have influence by the refractive index change of the GNPs surface due to the SPVD attachment to the GNPs [31]. As

a result, we confirm that vitamin D was successfully conjugated with GNPs.

The most popular synthetic method of generating GNPs is accomplished by using citrate reduction of $HAuCl_4$ in distilled water. This was introduced by Turkevich [24], and refined by Frens [25]. The benefits of this method are ease of production and simplicity of the process [15]. The various usages of GNPs are a result of their special property which enables surface modifications. Typically, GNPs surfaces easily graft with thiolate base ligands [15]. Based on this theory, we used SPVD as the simplest synthetic product between the two materials for conjugation with vitamin D. Vitamin D is expected to be synergistic in osteogenic differentiation with GNPs.

PEGylation based on polyethylene glycol (PEG) chains is a well-known method in drug delivery that extends the blood circulation time and delivery efficiency of nanoparticles [23,32]. We used SPVD for conjugation with GNPs (Figure 1(a)) as the GNPs can form a solid connection with the – SH group through the reaction formula displayed in Figure 1(b).

Understanding the uptake of particles by cells is crucial for control of intracellular drug delivery [33]. Endocytosis is the process of eukaryotes where extracellular components are absorbed into cells by formation of plasma membrane vesicles to surround these substances [34]. We evaluated the cellular uptake of both GNPs and VGNPs with the concentration fixed at 20 µM (Figure 4). In the cells, GNPs seemed to aggregate more than VGNPs as determined by FE-TEM (Figure 2(a)). In hADSCs, the GNPs' uptake ratio was found to be significantly higher than VGNPs. These results were explained by the difference in sizes between GNPs and VGNPs. Chithrani et al. [35] reported that both 30 and 50 nm GNPs showed greater uptake in mammalian cells as compared to 75 nm GNPs. In addition, Ko et al. [28] presented similar results that GNPs greater than 50 nm showed less cellular uptake in hADSCs as compared to smaller particles. The fabricated VGNPs had an average size of 60 nm (Table 2) which reduced the cellular uptake as compared to bare GNPs. Paradoxically, VGNPs showed less intracellular uptake than GNPs in comparison to the same area, however, they appear to have greater efficiency with higher osteogenic differentiation effects than GNPs (Figures 3(b), 5, 6).

A cytotoxicity test was performed to ensure that the concentration of GNPs and SPVD was appropriate (Supplementary Figures 1(a) and 2(a)). GNPs showed no cytotoxicity in the concentration range of 20–200 µM after 7 days of culture (Supplementary Figure 1). There was no significant cytotoxicity for SPVD between 1 and 100 µM (Supplementary Figure 2(a)). ALP, which is an early osteogenic differentiation marker, was found in the cell cultures due to osteogenic effects of GNPs and SPVD. At 14 days of culture, the 20 µM GNPs treated group showed higher ALP expression than others (Supplementary Figure 1(b)). Furthermore, the 20 µM SPVD treated group displayed significantly higher ALP expression levels than other concentrations of the SPVD treated groups. Therefore, we decided to synthesize a 1:1 ratio of VGNPs with a fixed concentration of 20 µM to confirm ALP activity. The ALP level commonly reaches it maximum at days 10–12 during osteogenesis [36]. The VGNPs group demonstrated significantly higher ALP expression at 10 days of culture as compared to others. It was found to be significantly increased as compared to control and GNPs at 15 days of culture as well. The

VGNPs presented less of an impact on ALP activity than the SPVD treated group. However, VGNPs showed greater mineralization levels of calcium deposition (Figure 5) assessed by alizarin red staining which allows for direct determination of mineralization [37]. At 3 weeks of culture, the VGNPs treated groups showed statistically higher amounts of calcium deposition than other groups (Figure 5(b)). These results indicate that VGNPs lead to osteogenic differentiation. To confirm with more analytical observation of VGNPs, we performed mRNA expression of COL1, OPN, BMP-2, and BSP by real-time PCR (Figure 6). At all time periods, VGNPs displayed higher expression levels of all osteogenic markers. In Figure 6(c), VGNPs showed a maximum at 2 weeks for expression of BMP-2. BMP-2 expression decreased at 3 weeks. BMP-2 plays a critical role in the differentiation of mesenchymal stem cells into osteoblasts [38]. Moreover, this data also matched both COL1, an abundant extracellular protein of bone produced by osteoblasts (Figure 6(a)), and OPN, an extracellular structural protein and organic component of bone, expressions (Figure 6(b)) at 2 weeks. BMP-2 induces the activation of OPN promoter typically at the 2 week time-point [39]. This result would explain the high OCN expression of VGNPs at 10 days (Figure 7) due to BMP-2 induces OCN expression. These results support that MAPKs are involved in BMP-2-induced osteoblast differentiation [38]. Collectively, it seems that VGNPs affect the activation of the MAPK signaling pathway which leads to BMP-2-induced osteogenic differentiation of hADSCs.

5. Conclusions

In summary, we fabricated GNPs by using the citrate reduction method. The fabricated GNPs were then conjugated to Thiol-PEG-Vitamin D with strong chemical bonding. In the cell viability test, the VGNPs demonstrated no cytotoxicity towards human adipose-derived stem cells at the concentrations tested. In the *in vitro* study, a concentration of 20 µM VGNPs was found to be effective at enhancing osteogenic differentiation. In particular, VGNPs displayed the highest expression levels for all osteogenic markers as determined by real-time PCR. Based on these results, VGNPs can be applied as powerful carriers that enhance osteogenic differentiation. The results of this study might help designing a nanoparticle system for treatment of osteoporosis in the bone tissue engineering field.

Disclosure statement

ORCID

Haram Nah http://orcid.org/0000-0003-3807-5166
Donghyun Lee http://orcid.org/0000-0003-0723-7505
Jae Seo Lee http://orcid.org/0000-0002-8266-8885
Sang Jin Lee http://orcid.org/0000-0002-8007-8785
Dong Nyoung Heo http://orcid.org/0000-0002-7717-7184
Ho-Jin Moon http://orcid.org/0000-0002-8056-5313
Il Keun Kwon http://orcid.org/0000-0001-9649-3003

References

[1] Burg KJ, Porter S, Kellam JK. Biomaterial developments for bone tissue engineering. Biomaterials. 2000;21:2347–2359.

[2] Kretlow JD, Mikos AG. Mineralization of synthetic polymer scaffolds for bone tissue engineering. Tissue Eng. 2007;13:927–938.

[3] Li W, Hou S, Yu B, et al. Genetics of osteoporosis: accelerating pace in gene identification and validation. Hum Genet. 2010;127:249–285.

[4] Abrahamsen B, Osmond C, Cooper C. Life expectancy in patients treated for osteoporosis: observational cohort study using national danish prescription data. J Bone Miner Res. 2015;30:1553–1559.

[5] Dawson-Hughes B, Harris SS, Krall EA, et al. Effect of calcium and vitamin D supplementation on bone density in men and women 65 years of age or older. N Engl J Med. 1997;337:670–676.

[6] Brommage R, Deluca HF. Evidence that 1, 25-dihydroxyvitamin D3 is the physiologically active metabolite of vitamin D3. Endocr Rev. 1985;6:491–511.

[7] DeLuca HF. Overview of general physiologic features and functions of vitamin D. Am J Clin Nutr. 2004;80:1689S–1696S.

[8] Allard L, Demoncheaux N, Machuca-Gayet I, et al. Biphasic effects of vitamin D and FGF23 on human osteoclast biology. Calcif Tissue Int. 2015;97:69–79.

[9] Wagner CL, Greer FR. Prevention of rickets and vitamin D deficiency in infants, children, and adolescents. Pediatrics. 2008;122:1142–1152.

[10] Song I, Kim B, Kim C, et al. Effects of BMP-2 and vitamin D_3 on the osteogenic differentiation of adipose stem cells. Biochem Biophys Res Commun. 2011;408:126–131.

[11] Piek E, Sleumer LS, van Someren EP, et al. Osteotranscriptomics of human mesenchymal stem cells: accelerated gene expression and osteoblast differentiation induced by vitamin D reveals c-MYC as an enhancer of BMP2-induced osteogenesis. Bone. 2010;46:613–627.

[12] Ramalho MJ, Coelho MA, Pereira MC. Anonymous a critical evaluation of vitamin D-clinical overview. London (UK): InTech; 2017.

[13] Cho K, Wang X, Nie S, et al. Therapeutic nanoparticles for drug delivery in cancer. Clin Cancer Res. 2008;14:1310–1316.

[14] Ghosh P, Han G, De M, et al. Gold nanoparticles in delivery applications. Adv Drug Deliv Rev. 2008;60:1307–1315.

[15] Daniel M, Astruc D. Gold nanoparticles: assembly, supramolecular chemistry, quantum-size-related properties, and applications toward biology, catalysis, and nanotechnology. Chem Rev. 2004;104:293–346.

[16] Salata OV. Applications of nanoparticles in biology and medicine. J Nanobiotechnology. 2004;2:3.

[17] Giljohann DA, Seferos DS, Daniel WL, et al. Gold nanoparticles for biology and medicine. Angew Chem. 2010;49:3280–3294.

[18] Gupta A, Moyano DF, Parnsubsakul A, et al. Ultrastable and biofunctionalizable gold nanoparticles. ACS Appl Mater Interfaces. 2016;8:14096–14101.

[19] Ali MR, Wu Y, Ghosh D, et al. Nuclear membrane-targeted gold nanoparticles inhibit cancer cell migration and invasion. ACS Nano. 2017;11:3716–3726.

[20] Sperling RA, Gil PR, Zhang F, et al. Biological applications of gold nanoparticles. Chem Soc Rev. 2008;37:1896–1908.

[21] Lee D, Heo DN, Lee SJ, et al. Poly (lactide-co-glycolide) nanofibrous scaffolds chemically coated with gold-nanoparticles as osteoinductive agents for osteogenesis. Appl Surf Sci. 2018;432:300–307.

[22] Heo DN, Ko W, Bae MS, et al. Enhanced bone regeneration with a gold nanoparticle–hydrogel complex. J Mater Chem B. 2014;2:1584–1593.

[23] Chen J, Guo Z, Tian H, et al. Production and clinical development of nanoparticles for gene delivery. Mol Ther Methods Clin Dev. 2016;3:16023.

[24] Turkevich J, Stevenson PC, Hillier J. A study of the nucleation and growth processes in the synthesis of colloidal gold. Discuss Faraday Soc. 1951;11:55–75.

[25] Frens G. Controlled nucleation for the regulation of the particle size in monodisperse gold suspensions. Nat Phys Sci. 1973;241:20.

[26] Boisselier E, Astruc D. Gold nanoparticles in nanomedicine: preparations, imaging, diagnostics, therapies and toxicity. Chem Soc Rev. 2009;38:1759–1782.

[27] Yi C, Liu D, Fong C, et al. Gold nanoparticles promote osteogenic differentiation of mesenchymal stem cells through p38 MAPK pathway. ACS Nano. 2010;4:6439–6448.

[28] Ko W, Heo DN, Moon H, et al. The effect of gold nanoparticle size on osteogenic differentiation of adipose-derived stem cells. J Colloid Interface Sci. 2015;438:68–76.

[29] Lee D, Heo DN, Nah HR, et al. Injectable hydrogel composite containing modified gold nanoparticles: implication in bone tissue regeneration. Int J Nanomedicine. 2018;13:7019.

[30] Gaumet M, Vargas A, Gurny R, et al. Nanoparticles for drug delivery: the need for precision in reporting particle size parameters. Eur J Pharm Biopharm. 2008;69:1–9.

[31] Tomaszewska E, Soliwoda K, Kadziola K, et al. Detection limits of DLS and UV-Vis spectroscopy in characterization of polydisperse nanoparticles colloids. J Nanomater. 2013;2013:60.

[32] Veronese FM, Pasut G. PEGylation, successful approach to drug delivery. Drug Discov Today. 2005;10:1451–1458.

[33] Alkilany AM, Murphy CJ. Toxicity and cellular uptake of gold nanoparticles: what we have learned so far? J Nanopart Res. 2010;12:2313–2333.

[34] Oh J, Choi S, Kim S, et al. Cellular uptake mechanism of an inorganic nanovehicle and its drug conjugates: enhanced efficacy due to clathrin-mediated endocytosis. Bioconjug Chem. 2006;17:1411–1417.

[35] Chithrani BD, Ghazani AA, Chan WC. Determining the size and shape dependence of gold nanoparticle uptake into mammalian cells. Nano Lett. 2006;6:662–668.

[36] Reddi AH. Role of morphogenetic proteins in skeletal tissue engineering and regeneration. Nat Biotechnol. 1998;16:247–252.

[37] Gregory CA, Gunn WG, Alexandra P, et al. An alizarin red-based assay of mineralization by adherent cells in culture: comparison with cetylpyridinium chloride extraction. Anal Biochem. 2004;329:77–84.

[38] Ryoo H, Lee M, Kim Y. Critical molecular switches involved in BMP-2-induced osteogenic differentiation of mesenchymal cells. Gene. 2006;366:51–57.

[39] Hullinger TG, Pan Q, Viswanathan HL, et al. TGFβ and BMP-2 activation of the OPN promoter: roles of Smad- and Hox-binding elements. Exp Cell Res. 2001;262:69–74.